Micromagnetic Computer Simulated Scaling Effect of S-Shaped Permalloy Nano-Element on Operating Fields for AND or OR Logic

Gavin S. Abo[1], Yang-Ki Hong[1], Byoung-Chul Choi[2], Michael J. Donahue[3], Seok Bae[1], Jeevan Jalli[1], Jihoon Park[1], Jaejin Lee[1], Mun-Hyoun Park[4], and Sung-Hoon Gee[5]

[1]Department of Electrical and Computer Engineering and MINT Center, The University of Alabama, Tuscaloosa, AL 35487 USA
[2]Department of Physics and Astronomy, University of Victoria, Victoria, BC V8W 3P6, Canada
[3]Mathematical & Computational Sciences Division, National Institute of Standards and Technology, Gaithersburg, MD 20899-8910 USA
[4]Hitachi Global Storage Technologies, San Jose, CA 95119-1003 USA
[5]Seagate Technologies, Bloomington, MN 55435 USA

The scaling effect of permalloy s-shaped element, a rectangular element with appendages, on operating fields, H_x and H_y, was investigated by micromagnetic computer simulations for AND or OR logic. The optimized combination of operating fields (H_x, H_y) was found to be $(27.7 \pm 9.9, -16.7 \pm 8.8)$, $(37.9 \pm 12.4, -25.9 \pm 6.0)$, and $(42.2 \pm 8.8, -23.9 \pm 4.0)$ in kA/m for the 100, 50, and 30 nm long s-shaped elements, respectively. As the s-shaped element is scaled down, the allowable deviation from the optimized operating fields becomes smaller and optimized operating fields shift to higher field.

Index Terms—Micromagnetic computer simulation, s-shaped element, spin logic.

I. INTRODUCTION

HYBRID complementary metal oxide semiconductor (CMOS)/magnetic architectures, where both magnetic memory and logic are integrated with CMOS, are potential candidates for next generation devices due to advantages such as nonvolatility and low power consumption [1]. Accordingly, there is a need for nano-sized logic elements or devices. Recently, the s-state magnetization configuration in magnetic element [2] has gained interest for nonvolatile, programmable magnetic logic device applications. Hesjedal *et al.* proposed the s-shaped permalloy element in Fig. 1, in which the magnetic element geometry stabilizes the s-state magnetization configuration. This element was studied by micromagnetic computer simulations for AND or OR logic devices [3]. The element shape is a rectangle with appendages. To retain the s-state magnetization, it was reported [3] that the s-shaped element geometry must: 1) not approach a square shape in the central part of the element as nucleation of a vortex occurs and 2) not have appendages too small compared to the overall element size. The logic inputs are set to the element by the combination of two orthogonal magnetic applied fields, H_x and H_y, in the x- and y-directions, respectively. The output is retrieved by reading the direction of the magnetization of the element using a magnetic tunnel junction (MTJ) or spin-valve structure.

In regards to spin logic devices, Allwood *et al.* fabricated the L-shaped element and demonstrated its AND or OR logic functionality [4] similar to the s-shaped element. On the other hand, magnetic quantum-dot cellular automata (MQCA) systems [5] and magnetic domain wall logic [6] have been demon-
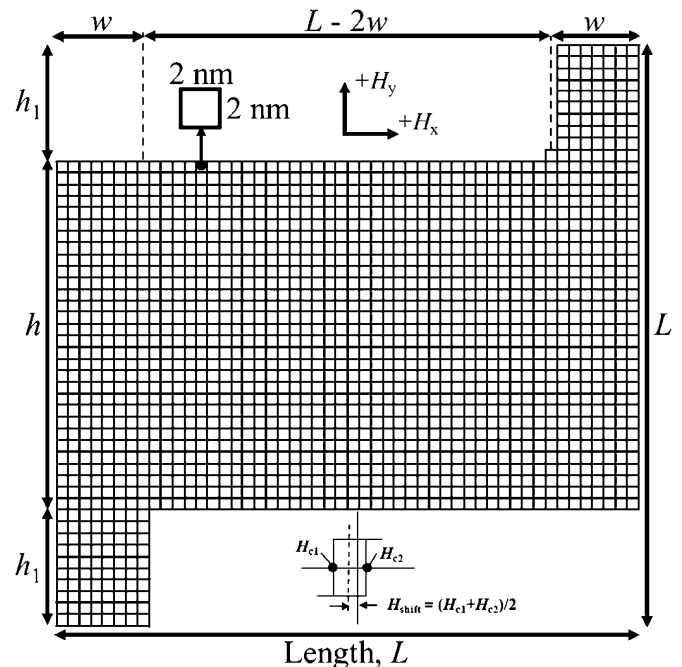

Fig. 1. Geometrical description of the 10 nm thick s-shaped element (top-view), where cells are cubes of $2 \times 2 \times 2$ nm^3 and element length is 100 nm. Definitions of fields are defined in the inset.

strated, but MQCA logic architecture requires more than one magnetic element of nm-size (20 quantum dots for AND) [7] and domain wall logic structure in the shape of a Y is on the relatively large hundred-nm scale. It has also been shown that small out-of-plane magnetization coupled to in-plane magnetization in α-MnAs thin films can be used for logic as magnetization reversal can be achieved by both in-plane and out-of-plane magnetic fields [8]. The magnetization coupling may be linked to the s-state magnetization configuration that was observed by magnetic force microscopy in the basal plane, while Landau, diamond, and double-diamond domain states were also observed

in the same film [9]. Moreover, application of α-MnAs thin film could be restricted by its material rather than shape properties. Alternatively, spin logic with MTJ and spin-valve based structures have been reported [10]–[13], but the s-shaped element can reduce the number of inputs or does not require a refresh terminal [14]. In other words, it uses both orthogonal lines whereas additional input lines are needed for MTJ and spin-valve based logic structures. Spin-transfer torque logic has been simulated [15], but patterning of the middle contact is expected to be difficult, thereby limiting its scaling.

The scalability of the s-shaped element and marginality in magnetic operating fields were not investigated for the recently reported logic device [3]. Accordingly, in this paper, we report the scaling effect of s-shaped permalloy nano-element on magnetic operating fields. Micromagnetic computer simulations were performed on 100 nm, 50 nm, and 30 nm long s-shaped elements to determine the operating fields. To find the optimized operating fields, the coercivities for magnetic fields applied in the x-direction, H_x, were obtained for different bias fields, H_{bias}. It is also shown that the cell size of 5 nm used for simulation of the 200 nm length in [3] may be too large for modeling the 200 nm length s-shaped element.

II. MICROMAGNETIC COMPUTER SIMULATION

The LLG micromagnetic simulator v2.63b [16] with predictor-corrector method was used to investigate the scalability of the s-shaped permalloy ($Ni_{80}Fe_{20}$) element. The following parameters for permalloy were used: saturation magnetization M_s of 800 kA/m, exchange stiffness A of 1.05×10^{-11} J/m, first uniaxial anisotropy constant K_{u1} of 100 J/m^3 aligned in the x-direction, and damping parameter α of 0.01. The mask for the s-shaped element of length $L = 100$ nm was defined to have heights $h = 60$ nm and $h_1 = 20$ nm, appendage width $w = 15$ nm, and cubic cell sizes of 2 nm and 5 nm. The element with 2 nm cell size is shown in Fig. 1. For the study of smaller s-shaped elements, all in-plane dimensions were scaled to $L = 50$ nm and 30 nm. In all cases, the thickness t was 10 nm. The $L = 50$ nm case was simulated with 5 nm and 2 nm cubic cells, while the $L = 30$ nm case was simulated with 2 nm and 1 nm cubic cells. It is noted that all cell sizes are less than the magnetostatic exchange length, ~ 5.1 nm ($l_{ex} = \sqrt{2A/(\mu_0 M_s^2)}$ in meters and SI units for soft magnetic material [17]). The appendage width for elements of $L = 30, 50,$ and 100 nm increased or decreased slightly off dimension when the shape's image was imported in order to fill or unfill whole cells. The masks with slight end shape variation, such as in Fig. 1, were used for the simulations. Coercivities were obtained from the hysteresis loops with nonuniform points by sweeping H_x from 159 to -159 kA/m, and back to 159 kA/m, at a fixed H_y called H_{bias}.

III. RESULTS AND DISCUSSION

Fig. 2 shows H_{bias} dependence of coercivities (H_{c1}, H_{c2}), which were extracted from the hysteresis loops (not shown). The application of H_y to the s-shaped element causes a shift in the hysteresis loop. The shift in field from the origin is the offset H_{shift}, defined in the inset loop of Fig. 1, where $H_{shift} = (H_{c1} + H_{c2})/2$. The shift is caused by the applied H_y and
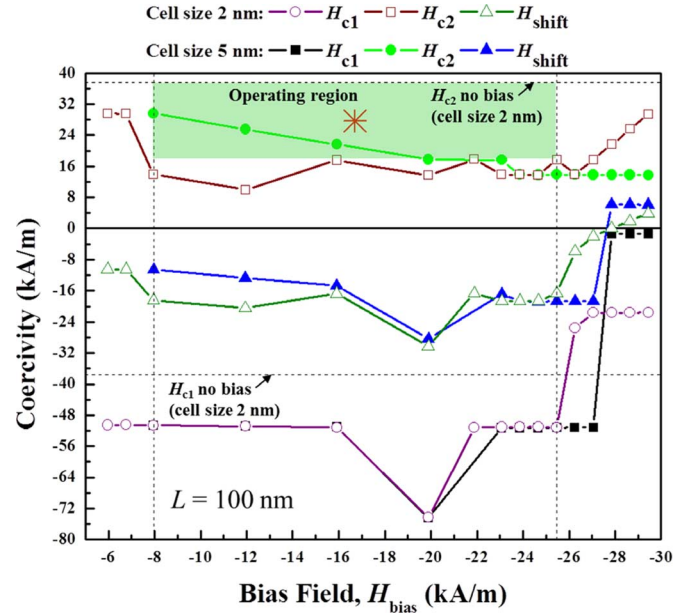

Fig. 2. Coercivities versus bias field plot for 100 nm long s-shaped element (lines guide the eye).

shape anisotropy holding the magnetization, since magnetization prefers to align in the direction of the applied field and along the length of the appendages, respectively. This is different and should not be confused with the exchange bias of ferromagnetic (FM) and antiferromagnetic (AFM) bilayer films, where the magnetization is held by exchange coupling between the FM and AFM layers.

For logic operation, the $+H_x$ must be larger than $+H_{c2}$ at $-H_{bias}$ and smaller than $+H_{c2}$ with no bias field, otherwise the magnetization will not switch or switch, respectively, resulting in loss of logic functionality. In addition, the $-H_{c1}$ at $-H_{bias}$ should be larger than $-H_x$ to avoid undesirable magnetization reversal. The $-H_{c1}$ at $-H_{bias}$ must also be greater than $-H_{c1}$ with no bias. Furthermore, the coercivities should be minimized, predictable, and remain about the same for variation in H_{bias}. The optimized operating field is the operating field between these ranges and in the center of the shaded operating region in Fig. 2. The coercivities for zero bias field ($H_{bias} = 0$ kA/m) were also obtained from hysteresis loops.

The optimized H_x is found to be $27.7 (= (37.6 + 17.8)/2) \pm 9.9 (= 37.6 - 27.7)$ kA/m, while the optimized H_y is $-16.7 (= (H_{bias,lower} + H_{bias,upper})/2 = -(25.5 + 7.96)/2) \pm 8.8$ kA/m for the 100 nm long s-shaped element for cell size of 2 nm. The simulations of the same element with cell size of 5 nm indicate that the cell size has a slight effect on the simulated coercivities. The asterisk in Fig. 2 represents the optimized point (H_x, H_y).

With regard to the scaled 50 nm long s-shaped element, the coercivities versus H_{bias} plot is shown in Fig. 3. The optimized combination of operating fields (H_x, H_y) is found to be $(37.9 \pm 12.4, -25.9 \pm 6.0)$ kA/m for cell size of 2 nm. There is a slight effect on coercivities when compared to the results for cell size of 5 nm as shown. Fig. 4 shows the coercivities versus H_{bias} plot for further scaled 30 nm long s-shaped element, and the optimized combination of operating fields is $(42.2 \pm 8.8, -23.9 \pm 4.0)$ kA/m for cell size of 1 nm. The differences in coercivities
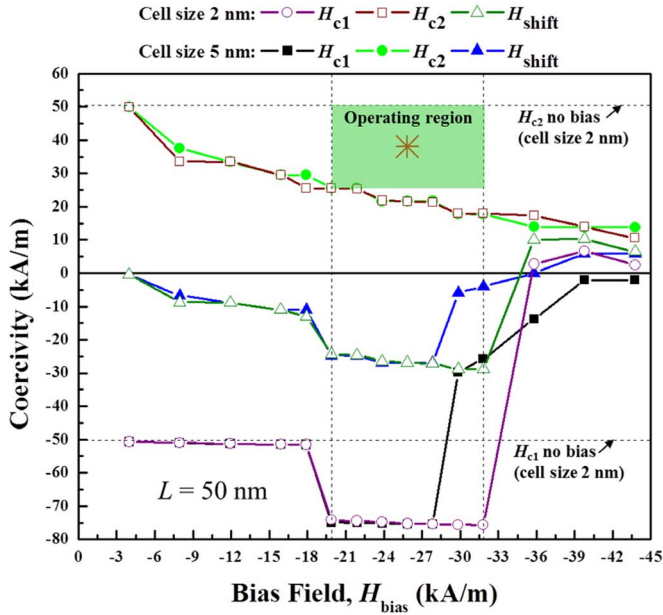
Fig. 3. Coercivities versus bias field plot for 50 nm long s-shaped element (lines guide the eye).
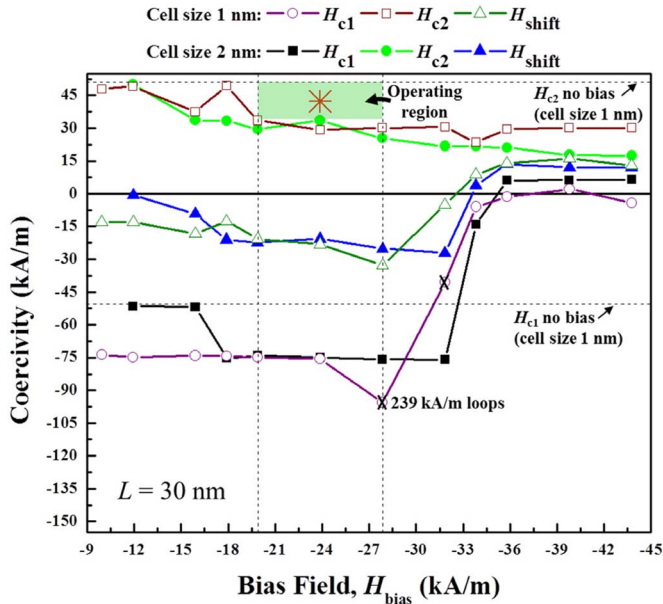

Fig. 4. Coercivities versus bias field plot for 30 nm long s-shaped element (lines guide the eye).

are small between the 2 nm and 1 nm cell sizes. This indicates convergence of the simulated results. A cell size equal to or less than 1 nm should therefore be used to obtain accurate coercivity. For the 100 and 50 nm length elements, the cell size should be equal to or less than 2 nm.

For the 30 nm length element with cell size of 1 nm, the coercivities at H_{bias} of -27.9 and -31.8 kA/m were obtained from the hysteresis loops with nonuniform points by sweeping H_x between 239 and -239 kA/m. This is because the H_x field of magnitude 159 kA/m was not high enough at H_{bias} of -27.9 and -31.8 kA/m to saturate the magnetization of the element.

The results (2 nm cell size for 100 and 50 nm, 1 nm cell size for 30 nm element) are combined in Fig. 5. This shows the s-shape
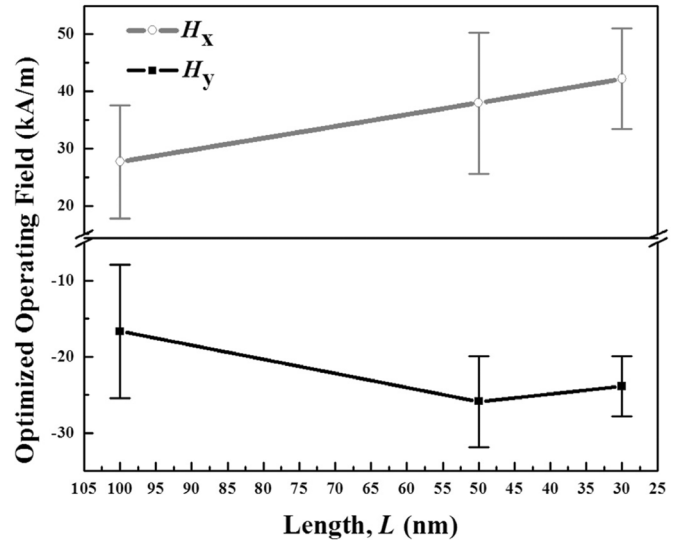

Fig. 5. S-shaped element length versus optimized operating fields (lines guide the eye). The bars from the points show amount of allowable deviation in optimized operating field.

TABLE I
TRUTH TABLE OF AND LOGIC FOR S-SHAPED ELEMENT OF DIFFERENT LENGTHS

AND	Input A (H_x in kA/m)			Input B (H_y in kA/m)			Output	
Length, L (nm)	100	50	30	100	50	30		
PRESET:	0	-27.7	-37.9	-42.2	0	+16.7	+25.9	+23.9	0	$-M_x$
$-M_x$	0	-27.7	-37.9	-42.2	1	-16.7	-25.9	-23.9	0	$-M_x$
←	1	+27.7	+37.9	+42.2	0	+16.7	+25.9	+23.9	0	$-M_x$
	1	+27.7	+37.9	+42.2	1	-16.7	-25.9	-23.9	1	$+M_x$

element length versus optimized H_x and H_y. The amount of allowable deviation in optimized operating field is given by the bars from the points. The allowable deviation in operating fields becomes smaller with decreasing element size, except for the operating range in H_x of the 50 nm length element, which is larger. In addition, operating fields shift to higher field as the s-shaped element is scaled down from 100 to 30 nm in length, except at 30 nm the optimized H_y drops slightly to negative 23.9 kA/m. The drop in optimized H_y for the element less than 50 nm in length may be due to relatively large aspect ratio of thickness to length (~ 0.3 for 30 nm length s-shaped element). The resulting truth table of AND logic for the s-shaped element of different lengths is given as Table I. As an example for AND logic, only the combination of optimized fields $(+27.7, -16.7)$ kA/m for element of 100 nm length is larger than the coercivity to cause complete magnetization reversal. All other 100 nm long element field combinations in the table do not change M_x, which is made possible by the shift in the hysteresis loop. The OR logic is achieved by setting the preset magnetization in the opposite direction.

With regards to the physical patterning limit for an s-shaped element, an estimate is made as follows. The ratio of h/w, the height h of the center rectangle to width w of the appendage, is $4 (= 60 \text{ nm}/15 \text{ nm})$ for the 100 nm length s-shaped element. Therefore, when the appendages reach the physical patterning limit, such as 13 nm for extreme ultraviolet lithography [18], the s-shaped element must be four times larger than a patterned 13 nm element. Accordingly, the patterning of the s-shaped element's appendages might limit the logic devices scalability.
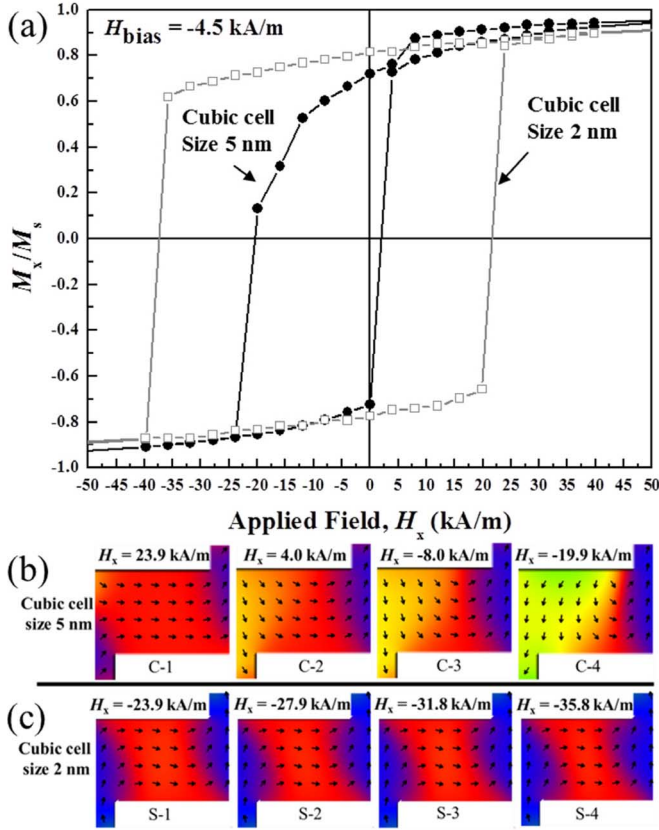
Fig. 6. (a) Normalized hysteresis loop of 200 nm long s-shaped element for cubic cell size of 5 and 2 nm at bias field of -4.5 kA/m, and $+M_x/M_s$ snapshots for corresponding (b) 5 nm and (c) 2 nm cubic cell size.

Fig. 7. (a) Normalized hysteresis loop of 100 nm long s-shaped element for cubic cell size of 2 nm at bias fields of -15.9, -19.9, and -23.9 kA/m and $+M_x/M_s$ snapshots for corresponding bias fields of (b) -15.9 kA/m and (c) -23.9 kA/m.

Moreover, thermal stability becomes an important factor as the magnetic nano-element shrinks. Hao *et al.* used Sharrock's equation to fit experimental temperature dependence of coercivity of rectangular elements. They concluded that $Ni_{19}Fe_{81}$ elements smaller than 150 nm $\times$ 230 nm $\times$ 1 nm (total volume 3.45×10^4 nm^3) would be superparamagnetic [19]. For the s-shaped elements considered in this work, the thermal barrier to switching can be estimated by tracking the change in the magnetic configuration energy along the hysteresis loop. It is found that the $L = 100$ nm element is stable with room temperature barrier height of $90k_B T_{300}$ (k_B is the Boltzmann constant and $T_{300} = 300$ K) at zero field and $75k_B T_{300}$ with a -16.7 kA/m bias field. However, the $L = 50$ nm and $L = 30$ nm elements are not thermally stable with energy barriers at zero field of not more than $24k_B T_{300}$ and $9.8k_B T_{300}$, respectively. This corresponds to median times-to-switch of 18.4 s and 12 μs, respectively. A comparison of these energy barriers against the coercive fields at zero bias fields yields effective activation volumes of 27%, 25%, and 32% of the $L = 100$ nm, 50 nm, and 30 nm elements, respectively. Thermal stability may be enhanced by increasing either the activation volume or the coercivity (or both) of an element. Given here the limited scope for increase in the activation volume, it appears that improvements in thermal stability for the $L = 50$ nm and 30 nm parts would necessitate increases in H_c.

Simulation cell size effects on an s-shaped element with $L = 200$ nm were also examined. The s-shaped element was scaled up from the 100 nm simulation parameters. The normalized hysteresis loops of the 200 nm long s-shaped element for cubic cell
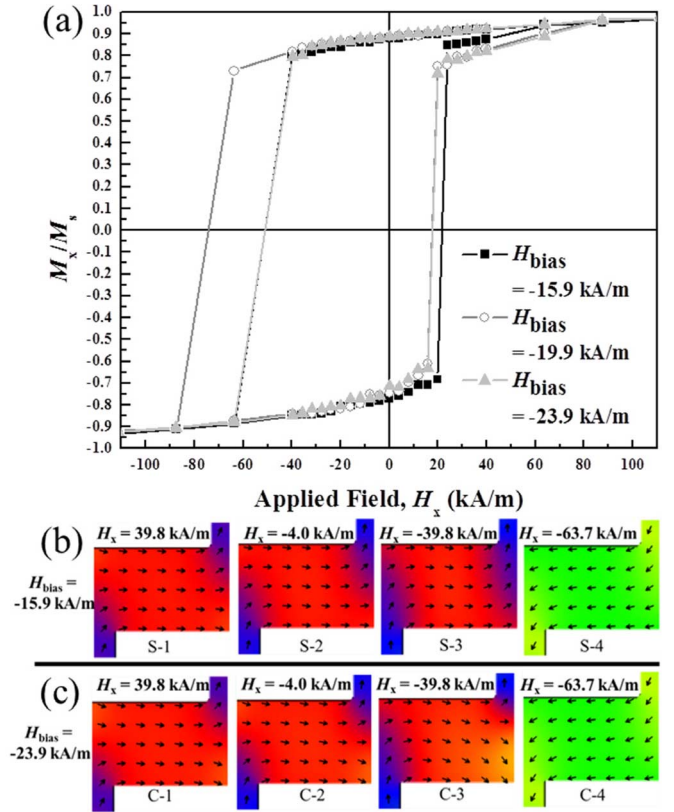
size of 5 nm and 2 nm at $H_{bias} = -4.5$ kA/m are shown in Fig. 6(a). The loss of squareness in the loop of 5 nm cell size is caused by formation of c-state rather than s-state in the element during switching as seen in Fig. 6(b). The difference in energy between c-state and s-state is less than 0.2% [20]. The c-state results due to domain walls and vortices being pinned because the cell size is too large [21]. It is noted that Dotse *et al.* found that if the cell size is too large, then the most energetic portion of a vortex is lost at the intersection of the four computational cells [22].

As seen in snapshot C-1 of Fig. 6(b) for the 5 nm cubic cell size, the s-state switches to the c-state causing the kink in the hysteresis loop, then the c-state moves out of the element to the right from C-2 to C-4 before switching. For the 2 nm cubic cell size, the s-shaped element does not form the c-state as shown in Fig. 6(c). The s-state is maintained while two domain walls near the appendages move and collide with each other at the center of the element from S-1 to S-4, then the element switches.

In Fig. 2, a dip is observed in H_{c1} at a bias field of -19.9 kA/m. This is due to a change in switching mechanism. The hysteresis loops before, at, and after the dip for bias field of -15.9, -19.9, and -23.9 kA/m, respectively, are shown in Fig. 7(a) for the 100 nm long element with 2 nm cell size. The switching mechanism at the dip has the same behavior as before it, such as shown by the snapshots in Fig. 7(b) of the element for a bias field of -15.9 kA/m. The two domain walls near the appendages move and collide with each other at the center of the element from S-1 to S-3, and then, the element switches in S-4 when H_x is greater than H_{c1}. On the other hand, for bias

fields greater than -19.9 kA/m, it seems that the large bias field may be the cause of a c-state forming in the element as shown in Fig. 7(c) for the bias field of -23.9 kA/m. The domain in the left appendage is seen moving towards the center of the element and forms a c-state from C-1 to C-3. The domain in the right element is pushed up and out of the element before switching at H_{c1} and has switched in C-4.

IV. SUMMARY

It was confirmed by our simulation results that magnetic field switching of s-shaped magnetic elements may be suitable for application on large scale and low logic density. For 100, 50, and 30 nm long s-shaped permalloy elements, the optimized combination of operating fields were found to be $(27.7 \pm 9.9, -16.7 \pm 8.8)$, $(37.9 \pm 12.4, -25.9 \pm 6.0)$, and $(42.2 \pm 8.8, -23.9 \pm 4.0)$ in kA/m, respectively. The appendages of the s-shaped element were found to be a physical limitation to its scalability. As activation volume approaches the superparamagnetic limit, thermal stability of the magnetization in the element becomes an important consideration. Micromagnetic simulations imply that the 100 nm s-shaped element is thermally stable at room temperature, but not the 50 or 30 nm elements. It appears that increasing the thermal stability of the smaller parts would entail an increase in their operating fields. For micromagnetic simulations, the choice of cell size can be critical when there are c- and s-states in the magnetization reversal. Smaller cell sizes should be used, but come at a cost of longer computational time. Finally, spin-torque switching of the s-shaped element at nano-scale remains to be investigated.

ACKNOWLEDGMENT

REFERENCES

[1] G. Prenat, B. Dieny, W. Guo, M. El Baraji, V. Javerliac, and J. P. Nozières, "Beyond MRAM, CMOS/MTJ integration for logic components," *IEEE Trans. Magn.*, vol. 45, no. 10, pp. 3400–3405, Oct. 2009.

[2] X. Liu, J. N. Chapman, S. McVitie, and C. D. W. Wilkinson, "Introduction and control of metastable states in elliptical and rectangular magnetic nanoelements," *Appl. Phys. Lett.*, vol. 84, no. 22, pp. 4406–4408, 2004.

[3] T. Hesjedal and T. Phung, "Magnetic logic element based on an S-shaped permalloy structure," *Appl. Phys. Lett.*, vol. 96, no. 7, p. 072501, 2010.

[4] D. A. Allwood, N. Vernier, G. Xiong, M. D. Cooke, D. Atkinson, C. C. Faulkner, and R. P. Cowburn, "Shifted hysteresis loops from magnetic nanowires," *Appl. Phys. Lett.*, vol. 81, no. 21, pp. 4005–4007, 2002.

[5] A. Imre, G. Csaba, L. Ji, A. Orlov, G. H. Bernstein, and W. Porod, "Majority logic gate for magnetic quantum-dot cellular automata," *Science*, vol. 311, pp. 205–208, 2006.

[6] D. A. Allwood, G. Xiong, C. C. Faulkner, D. Atkinson, D. Petit, and R. P. Cowburn, "Magnetic domain-wall logic," *Science*, vol. 309, pp. 1688–1692, 2005.

[7] M. J. Beard, "Design and Simulation of Fault-Tolerant Quantum-Dot Cellular Automata (QCA) NOT Gates," M.S. thesis, Wichita State Univ., Wichita, KS, 2006.

[8] R. Koch, "Unusual magnetic properties of MnAs thin films: A new approach to magnetologic computing," *Physica E*, vol. 25, pp. 181–188, 2004.

[9] R. Engel-Herbert, T. Hesjedal, and D. M. Schaadt, "Three-dimensional micromagnetic domain structure of MnAs films on GaAs(001): Experimental imaging and simulations," *Phys. Rev. B*, vol. 75, p. 094430, 2007.

[10] A. Ney, C. Pampuch, R. Koch, and K. H. Ploog, "Programmable computing with a single magnetoresistive element," *Nature*, vol. 425, pp. 485–487, 2003.

[11] X. Yao, J. Harms, A. Lyle, F. Ebrahimi, Y. Zhang, and J. P. Wang, "Magnetic tunnel junction-based spintronic logic units operated by spin transfer torque," *IEEE Trans. Nanotechnol.*, vol. 11, no. 1, pp. 120–126, Jan. 2012.

[12] A. Lyle, X. Yao, F. Ebrahimi, J. Harms, and J. P. Wang, "Communication between magnetic tunnel junctions using spin-polarized current for logic applications," *IEEE Trans. Magn.*, vol. 46, no. 6, pp. 2216–2219, Jun. 2010.

[13] S. Lee, S. Choa, S. Lee, and H. Shin, "Magneto-logic device based on a single-layer magnetic tunnel junction," *IEEE Trans. Electron Devices*, vol. 54, no. 8, pp. 2040–2044, Aug. 2007.

[14] J. Shen, "Logic devices and circuits based on giant magnetoresistance," *IEEE Trans. Magn.*, vol. 33, no. 6, pp. 4492–4497, Nov. 1997.

[15] V. Höink, J. W. Lau, and W. F. Egelhoff, "Micromagnetic simulations of a dual-injector spin transfer torque operated spin logic," *Appl. Phys. Lett.*, vol. 96, no. 14, p. 142508, 2010.

[16] M. R. Scheinfein, LLG Micromagnetic Simulator™ [Online]. Available: http://llgmicro.home.mindspring.com

[17] M. J. Donahue and D. G. Porter, "Exchange energy formulations for 3D micromagnetics," *Physica B*, vol. 343, pp. 177–183, 2004.

[18] M. Totzeck, W. Ulrich, A. Göhnermeier, and W. Kaiser, "Semiconductor fabrication: Pushing deep ultraviolet lithography to its limits," *Nature Photon.*, vol. 1, pp. 629–631, 2007.

[19] Y. Hao, C. A. Ross, and H. I. Smith, "Thermal stability of the magnetization of 150 nm × 230 nm $Ni_{19}Fe_{81}$ elements," *J. Appl. Phys.*, vol. 93, no. 10, pp. 7909–7911, 2003.

[20] T. Schrefl, J. Fidler, J. N. Chapman, and K. J. Kirk, "Micromagnetic simulation of domain structures in patterned magnetic tunnel junctions," *J. Appl. Phys.*, vol. 89, no. 11, pp. 7000–7002, 2001.

[21] M. J. Donahue and R. D. McMichael, "Exchange energy representations in computational micromagnetics," *Physica B*, vol. 233, pp. 272–278, 1997.

[22] D. Dotse and A. S. Arrott, "Micromagnetic studies of vortices leaving and entering square nanoboxes," *J. Appl. Phys.*, vol. 97, no. 10, p. 10E307, 2005.